Mechanical fatigue of human red blood cells

Yuhao Qiang[a], Jia Liu[a], Ming Dao[b,1], Subra Suresh[c,1], and E. Du[a,d,1]

[a]Department of Ocean and Mechanical Engineering, Florida Atlantic University, Boca Raton, FL 33431; [b]Department of Materials Science and Engineering, Massachusetts Institute of Technology, Cambridge, MA 02139; [c]Nanyang Technological University, Republic of Singapore 639798; and [d]Department of Biological Sciences, Florida Atlantic University, Boca Raton, FL 33431

Contributed by Subra Suresh, August 15, 2019 (sent for review June 17, 2019; reviewed by Guruswami Ravichandran and M. Taher A. Saif)

Fatigue arising from cyclic straining is a key factor in the degradation of properties of engineered materials and structures. Fatigue can also induce damage and fracture in natural biomaterials, such as bone, and in synthetic biomaterials used in implant devices. However, the mechanisms by which mechanical fatigue leads to deterioration of physical properties and contributes to the onset and progression of pathological states in biological cells have hitherto not been systematically explored. Here we present a general method that employs amplitude-modulated electrodeformation and microfluidics for characterizing mechanical fatigue in single biological cells. This method is capable of subjecting cells to static loads for prolonged periods of time or to large numbers of controlled mechanical fatigue cycles. We apply the method to measure the systematic changes in morphological and biomechanical characteristics of healthy human red blood cells (RBCs) and their membrane mechanical properties. Under constant amplitude cyclic tensile deformation, RBCs progressively lose their ability to stretch with increasing fatigue cycles. Our results further indicate that loss of deformability of RBCs during cyclic deformation is much faster than that under static deformation at the same maximum load over the same accumulated loading time. Such fatigue-induced deformability loss is more pronounced at higher amplitudes of cyclic deformation. These results uniquely establish the important role of mechanical fatigue in influencing physical properties of biological cells. They further provide insights into the accumulated membrane damage during blood circulation, paving the way for further investigations of the eventual failure of RBCs causing hemolysis in various hemolytic pathologies.

mechanical fatigue of biological cells | mechanical fatigue of erythrocytes | fatigue-induced damage | cyclic loading | static loading

Fluctuations and repeated cyclic variations in mechanical loads or strains lead to the onset, subcritical growth, and eventual catastrophic failure of engineered materials (1). Deterioration of physical properties, structural integrity, and functional performance arising from this mechanical fatigue effect is a major consideration in the design of materials and components used in a wide spectrum of engineering applications including buildings, roads, bridges, and other civil infrastructure, aircraft, automotive parts, marine structures, pressure vessels, pipelines, and coatings used for thermomechanical protection. These considerations of mechanical fatigue have given rise to stringent guideline standards for the design and routine maintenance of human life-critical and safety-critical structures and components such as commercial passenger aircraft (1, 2). Practical implications of mechanical fatigue in daily life and its technological and economic consequences for industry and society have led to considerable scientific research over many decades into the mechanisms of cyclic deformation, fatigue crack initiation, subcritical flaw propagation, and final fracture in a wide variety of materials. These studies in engineering materials have demonstrated significantly more deleterious effects of cyclic loads on the creation and propagation of damage and cracking than those seen under sustained or monotonically varying loads or strains of the same maximum intensity imposed for the same duration of time (see, e.g., a comprehensive literature review of mechanisms, mechanics, and practical implications of fatigue in ref. 1). Exacerbation of damage evolution in metal alloys under fluctuating loads stems from to-and-fro motion of defects which typically leads to the localization of deformation around preferential crystallographic orientations, shear planes and directions, free surfaces, and sites of stress concentrators. This process is aided by continual changes in the underlying material structure and substructure to promote cycle-by-cycle accumulation of fatigue damage which advances subcritically until catastrophic fracture occurs (1).

Mechanical fatigue of engineering components used in load-bearing structures and its consequences in the presence of elevated or low temperatures, corrosive environments, irradiation, thermal fluctuations, and residual stresses have been the primary focus of scientific studies for more than a century (1). With advances in microelectronics and microelectromechanical systems, thermal fatigue and mechanical fatigue of thin films and multilayered materials have also evolved as a subject of scientific investigation for material design, reliability prediction, and analysis of the integrity of functional devices (3). More recently, numerous studies have identified the role of fatigue in influencing the structure, properties, and performance of natural and synthetic biomaterials as, for example, in the case of mineralized human tissues such as cortical bone and dentin (4), orthopedic (1) and dental implants (5), synthetic heart valves (6), and hydrogels (7) used in tissue engineering, personal care, and medicine.

Biological cells, such as human red blood cells (RBCs), undergo significant cyclic deformation through large elastic stretching and relaxation as they squeeze through and traverse microvasculature and other size-limiting pathways to perform their biological

Significance

The mechanisms underlying degradation of biological cells due to mechanical fatigue are not well understood. Specifically, detrimental effects of fatigue on properties and homeostasis of human red blood cells (RBCs), as they repeatedly deform while traversing microvasculature, have remained largely unexplored. We present a general microfluidics method that incorporates amplitude-modulated electrodeformation to induce static and cyclic mechanical deformation of RBCs. Fatigue of RBCs leads to significantly greater loss of membrane deformability, compared to static deformation under the same maximum load and maximum-load duration. These findings establish unique effects of cyclic mechanical deformation on the properties and function of biological cells. Our work provides a means to assess the mechanical integrity and fatigue damage of RBCs in blood circulation.

Author contributions: M.D., S.S., and E.D. designed research; Y.Q. and J.L. performed research; Y.Q., J.L., M.D., S.S., and E.D. analyzed data; and Y.Q., M.D., S.S., and E.D. wrote the paper.

Reviewers: G.R., California Institute of Technology; and M.T.A.S., University of Illinois at Urbana–Champaign.

The authors declare no conflict of interest.

[1]To whom correspondence may be addressed. Email: mingdao@mit.edu, ssuresh@ntu.edu.sg, or edu@fau.edu.

This article contains supporting information online at www.pnas.org/lookup/suppl/doi:10.1073/pnas.1910336116/-/DCSupplemental.

First published September 16, 2019.

function of oxygen transport during their typical lifespan of 120 d in the human body. Some medical devices such as synthetic heart valves can serve as additional mechanical challenges exacerbating fatigue damage and hemolysis of RBCs in circulation (8). Prior work has reported indirect measurement of deformation using shear flow of a population of cells in a microchannel (9) and observations of a reduction in deformability in RBC membranes as a result of static shear stresses (10, 11). However, systematic studies of mechanical fatigue at the single-cell level and experimental evidence for the occurrence of cyclic loading effects in biological cells have not been reported to date. Investigation of these issues is particularly significant because many of the models and mechanisms to characterize the mechanical properties of engineered materials, which are known to be severely susceptible to damage and failure by fatigue, are also widely adapted with appropriate modifications to describe the complex and clinically relevant mechanical behavior of biological cells in health and disease (12, 13).

There is thus a need for scientific investigations into mechanical fatigue to address the following fundamental questions:

First, what is the effect of fluctuations in stresses or deformation of a healthy biological cell on its mechanical and physical characteristics, structural integrity, and performance, as a function of such factors as the maximum intensity, amplitude and rate of strain, frequency of cyclic deformation, number of cycles, and so on?

Second, is the effect seen specific to cyclic variations in deformation? In other words, to what extent does it occur, by comparison, under static, quasi-static, or monotonic variations in deformation at comparable levels of maximum "intensity" of strain or stress for comparable durations of time?

In order to address these questions systematically, we choose the human RBC for the single-cell investigation. RBCs are highly specialized cells that are well adapted for respiratory gas exchange in the cardiovascular system. Their unique membrane structure, which comprises a lipid bilayer and a 2D cytoskeleton made of spectrin networks (14, 15), contributes to the intrinsic resilience of RBCs to withstand shear stresses induced by blood flow and repeated deformation exerted by physical constraints from capillaries and interendothelial slits (16). The absence of a nucleus and of a complex 3D cytoskeleton in the disk-shaped RBC further facilitates relatively easier analyses of cyclic deformation. In addition, as RBCs travel through blood vessels with variable vascular resistance (17) they are subjected to intermittent stresses and cyclic strains. During their lifespan, RBCs gradually lose their mechanical integrity (18), and senescent RBCs are eventually removed by splenic filtration (16). How the RBCs lose their mechanical integrity solely in response to cyclic deformation during their normal biological function is, therefore, a topic of considerable scientific and clinical interest. In certain infectious diseases (19, 20) and inherited blood disorders (21), survival of affected RBCs is remarkably reduced due to the abnormalities in cell membranes and the attendant changes in cell properties, and mechanical fatigue could contribute further to the loss of deformability of diseased cells.

In this work, we employed a unique and general experimental technique to investigate whether mechanical fatigue effects occur in biological cells and to address the foregoing fundamental questions that identify any possible role of mechanical fatigue in influencing the properties of RBCs. Our method employs amplitude-modulated electrodeformation in conjunction with microfluidics (22) (Fig. 1*A*) and is capable of imposing on the single RBCs controlled static loads for prolonged periods of time or large numbers of cyclically varying mechanical strains.

A sinusoidal carrier wave with a frequency of 1.58 MHz is selected for easy cell immobilization by positive dielectrophoresis (DEP) and electrodeformation (23). See *SI Appendix*, *Electro-Deformation Characterization of RBCs* for a summary of the principles underlying electrodeformation loading of RBCs and for details of experimental methods and sample preparation. *SI Appendix*, Fig. S1*A* graphically shows the rationale for the choice of a

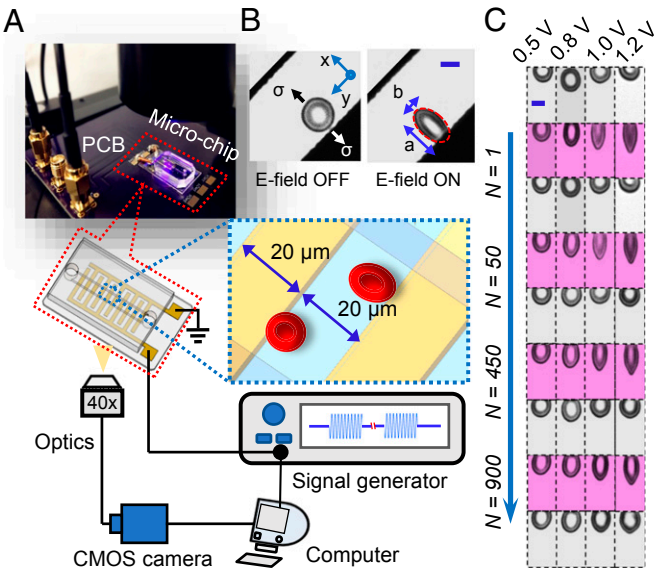

Fig. 1. Fatigue testing of single RBCs using amplitude-modulated electrodeformation. (*A*) Experimental setup for real-time measurement of cell deformation in a microfluidic chip. Schematic shows the key components of the testing system, including the microfluidic device with interdigitated microelectrodes, signal generator for producing modulated sinusoidal carrier wave, and computer for data acquisition, analysis, and modeling. (*B*) Microscopic images of a representative RBC when the electric field (E-field) is ON and OFF. Dimensions of RBC are measured along *x* and *y* axes (*a* and *b*, respectively). (*C*) Microscopic images of cell deformation at 4 representative loading levels arising from applied voltages of 0.5, 0.8, 1.0, and 1.2 V as functions of loading cycles (N = 1, 50, 450, and 900). (Scale bars in *B* and *C*, 5 μm.)

frequency of 1.58 MHz for the current experiments. *SI Appendix*, Fig. S1 *B–D* provide results of our parametric analysis of the effects of variations in cell membrane conductivity, cytoplasm permittivity, and cytoplasm conductivity, respectively, on the DEP response of RBCs. The freely suspended RBCs move toward the electrode edges by positive DEP and deform into a quasi-ellipsoid shape due to electrodeformation (Fig. 1*B*). Each RBC is individually tracked and analyzed.

Results

Morphological Characteristics of Fatigued RBCs. Cyclic tensile loading of constant amplitude was achieved by imposing a step-function voltage (rectangular waveform) to the carrier wave. The root-mean-square value of the voltage, which determines the peak load of the fatigue cycle, was fixed at 0.5, 0.8, 1.0, and 1.2 V. All of the voltage values reported in this paper refer to this root-mean-square voltage. Since the minimum voltage in the fully unloaded state is zero when the electrical input is fully turned off, the stress ratio or load ratio of the fatigue cycle, R, which is the ratio of the minimum to the maximum load (stress) of the fatigue cycle, is zero. A fixed time period of 4 s for cyclic loading and unloading, with 2 s for loading and 2 s for unloading, was used in the experiment (Movie S1). The cyclic loading frequency is thus 0.25 Hz with a rectangular waveform.

During the loading phase, cells rapidly deformed and attained an equilibrium between electrodeformation force and the resultant membrane elastic force in a finite period of time. This time period for deformation stabilized within 0.6 ± 0.2 s in the first fatigue cycle and it increased up to 1.5 ± 0.3 s after about 900 fatigue cycles, for all of the voltage levels. The RBCs gradually relaxed to their stress-free states during unloading, with the typical characteristic time for relaxation being 0.16 ± 0.04 s in the first cycle. Fig. 1*C* shows the time sequences of microscopic images of 4 representative

disk-shaped RBCs at the 4 voltages, for fatigue loading cycles $N = 1$, 50, 450, and 900. Regions highlighted in gray show cell shapes in the fully relaxed state and those in purple show the fully deformed state. Within the initial 50 cycles, cells were able to completely recover their initial disk shape upon unloading from the peak load. Permanent deformation in cell membranes started to occur only after about 450 fatigue cycles and continued for the remainder of cyclic loading. The extent of permanent deformation was higher at the higher voltages of 1.0 V and 1.2 V, as seen in Fig. 1*C*. Cell morphological change is quantified by the stretch ratio S_R, which is the ratio of the major axis, a, to the minor axis, b, of the cell fitted by an ellipse. Evolution of S_R values of 4 representative RBCs deformed by 0.5, 0.8, 1.0, and 1.2 V are plotted as functions of time, respectively (*SI Appendix*, Fig. S2 *A–D*). As seen in *SI Appendix*, Fig. S2, the time required for cells to attain a plateau in maximum S_R and the time for full relaxation extend significantly into many cycles of fatigue loading. These findings suggest that the deleterious effects of cyclic loads on RBC membrane damage are manifested only after a critical number of cycles and that they accumulate over hundreds of fatigue cycles. Permanent damage in cell membranes is consistently observed when the voltage level is in excess of 0.5 V. The characteristic features of fatigue damage in RBC membranes include pronounced shape changes from a disk shape into elliptocyte, stomatocyte, or knizocyte-like shapes, as well as the development of single to multiple thorny projections on cell membranes (*SI Appendix*, Fig. S2*E*).

Degradation in Mechanical Properties of RBCs. We characterized the mechanical properties of RBC membranes in response to different levels of shear stresses calibrated from different voltage values. Details of shear stress calibration can be found elsewhere (23). A brief description of our constitutive models for the viscoelastic deformation characteristics of RBCs and of the cell-membrane shear stresses is presented in *SI Appendix*, *Constitutive Model for Viscoelastic Deformation of RBC Membranes*. The applied voltage was kept at no more than 2.0 V to prevent any possible membrane damage that may occur outside of mechanical fatigue. For this reason, the loading was kept below certain threshold levels: a threshold electrical field strength of 2.1 kV/cm (24) and mechanical stress on the membrane of 150 Pa (25). For an assumed membrane thickness of 10 nm, the corresponding values of RBC membrane shear stresses were calculated to be 1.19 ± 0.22 Pa, 1.87 ± 0.42 Pa, 2.85 ± 0.77 Pa, 4.78 ± 1.48 Pa, and 9.63 ± 3.21 Pa for the applied voltages of 0.8, 1.0, 1.2, 1.5, and 2.0 V, respectively.

The dynamic deformation of RBCs is characterized by the transient value of the principal extension/contraction ratio, $\lambda(t)$, which is calculated by dividing the initial value of the minor axis, b_0, by its transient value, $b(t)$.* Fig. 2*A* shows the instantaneous value of λ as a function of number of fatigue cycles, N, for a particular

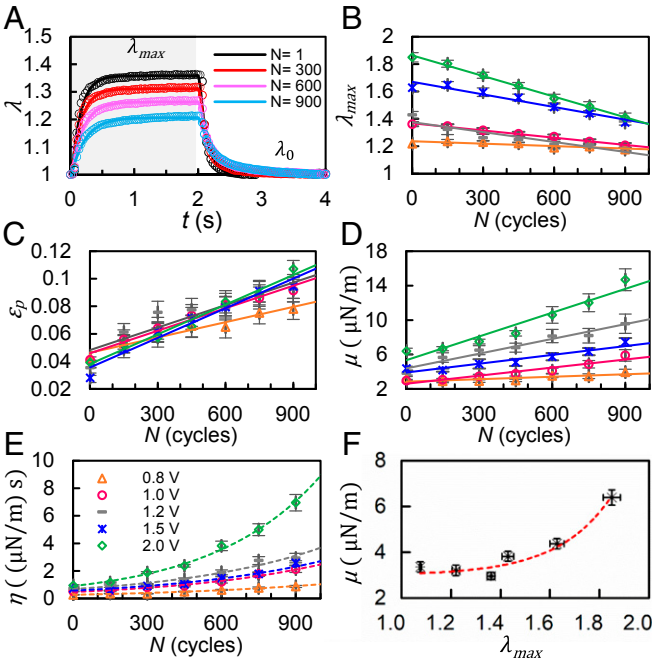

Fig. 2. Degradation of mechanical properties of RBCs under cyclic tensile loading of constant amplitude. (*A*) Instantaneous values of λ averaged from individually tracked cells ($n = 20$) in both stretching phase (gray region) and relaxation phase (white region) for $N = 1$, 300, 600, and 900 fatigue cycles at 1.0 V. Open circles represent experimental measurement and the solid curves represent exponential fit to the data. (*B–E*) Variation of the mean value of λ_{max}, ε_p, μ, and η, respectively, of RBCs with the number of fatigue loading cycles, N, for 5 different voltage levels of 0.8, 1.0, 1.2, 1.5, and 2.0 V (represented by the same set of symbols as shown in *E*). (*F*) Nonlinearity in membrane shear modulus, μ, plotted as a function of λ_{max} at $N = 1$. The solid lines represent the best fit linear regression lines. The dashed lines represent the best fit exponential curves. Error bars indicate standard error of the mean (SEM).

voltage of 1.0 V. Values of λ during the stretching phase and the relaxation phase can be fitted well with an exponential function, $\lambda = A \times \exp(B \times t) + C$, for each cycle. We extract the maximum extension ($\lambda_{\max}$) and the minimum extension (λ_0) in the fully stretched and fully relaxed states, respectively. The initial value of $\lambda_{\max}$ indicated by the vertical intercept ($\tilde{\lambda}_{\max}$) increases with the voltage level as a result of higher resulting stresses, with the best-fit linear regression, $\tilde{\lambda}_{\max} = 0.53 \times V + 0.82$, with $R^2 = 0.96$. Mean values of $\lambda_{\max}$ decrease from 1.36 for $N = 1$ to 1.32, 1.27, and 1.21 for $N = 300$, 600, and 900, respectively.

The value of $\lambda_{\max}$ strongly varies with the number of loading cycles for all stress levels. The best-fit linear regressions are $\lambda_{\max} = -8 \times 10^{-5} \times N + 1.25$ with $R^2 = 0.90$ for 0.8 V, $\lambda_{\max} = -2 \times 10^{-4} \times N + 1.37$, with $R^2 = 0.99$ for 1.0 V, $\lambda_{\max} = -2 \times 10^{-4} \times N + 1.38$, with $R^2 = 0.85$ for 1.2 V, $\lambda_{\max} = -3 \times 10^{-4} \times N + 1.67$, with $R^2 = 0.95$ for 1.5 V, and $\lambda_{\max} = -5 \times 10^{-4} \times N + 1.86$ with $R^2 = 1.0$ for 2.0 V, as shown in Fig. 2*B*. Additionally, the magnitude of the negative slope (m) of the lines decreases with increasing voltage, with the best-fit linear regression, $m = 3 \times 10^{-4} \times V - 2 \times 10^{-4}$, with $R^2 = 0.97$. These results indicate that the rate of mechanical damage of the cell membrane is proportional to the intensity of cyclic deformation which, in turn, depends on the magnitude of voltage.

In order to quantify and compare the extent of fatigue damage arising among the different cases, permanent deformation in RBC membrane during fatigue was evaluated by the effective plastic strain, $\varepsilon_p = (S_{R_{\min}}(N) - 1/S_{R_{\min}}(N))/4$, where $S_{R_{\min}}$denotes the minimum stretch ratio in fully relaxed state. The mean value of ε_p is proportional to the number of loading cycles ($R^2 > 0.9$; Fig. 2*C*). The slope of the linear functions increases with the voltage level,

*Note that $\lambda(t)$ is defined here in terms of the instantaneous value of the contraction ratio in the transverse direction of tensile cyclic loading, $b_0/b(t)$, rather than as the axial extension ratio, $a(t)/a_0$. This is because a small part of the deformed membrane along the tensile loading axis of axial dimension a is necessarily obstructed from view by the gold electrode when imaging the cell. This partial obstruction could lead to some error in the analysis of deformation if the latter definition of $\lambda(t)$ along the axial direction had been invoked. In *SI Appendix*, we demonstrate that the definition and choice of the instantaneous values of extension ratio based either on the axial extension ratio, $a(t)/a_0$, or the corresponding transverse contraction ratio, $b_0/b(t)$, has absolutely no effect on the trends discovered here about the role of mechanical fatigue in influencing the behavior of RBCs. There are, however, some anticipated differences in the quantitative values of key parameters characterizing mechanical fatigue effects between the 2 related definitions of actual values of $\lambda(t)$ because of the normal variations in cell response in this mutually orthogonal directions and the experimental scatter and errors in extracting axial and transverse dimensions during deformation from optical images. Because of the relatively greater accuracy of the former definition, $\lambda(t) = b_0/b(t)$, in the experimental measurements, all subsequent results on the principal extension ratio are presented in the paper, with this choice of definition. For completeness, we present all of the corresponding results obtained using the alternative definition of axial extension ratio, $a(t)/a_0$, in *SI Appendix* and demonstrate that none of the trends and conclusions reported here is unaffected by the particular choice of the definition of the extension ratio.

suggesting that plastic strain accumulation occurs faster at higher voltage levels.

The viscoelastic characteristics of RBC membranes, including shear modulus and shear viscosity, vary significantly with the number of fatigue cycles (Fig. 2 *D* and *E*). For instance, at 1.2 V, the mean values of shear modulus increase from 3.82 μN/m in the first fatigue cycle to 9.58 μN/m for the 900th fatigue cycle. This is quantified with a linear regression analysis, $\mu = 5.7 \times 10^{-3} \times N + 4.4$ with $R^2 = 0.95$. In the first cycle, the shear modulus ranges from 3.2 ± 0.2 μN/m at 0.8 V to 6.4 ± 0.4 μN/m at 2.0 V. The nonlinear variation here of membrane shear modulus with the maximum extension ratio (Fig. 2*F*) is consistent with trends reported by previous studies for static deformation (26, 27). The mean value of membrane shear moduli measured at all voltage levels is 4.1 ± 1.4 μN/m, which is within the range of values in the literature, 1.8 to 11.3 μN/m, for healthy RBC membranes, from a number of independent studies that employ different experimental methods (28–30).

The membrane shear viscosity, η, was determined by multiplying the characteristic relaxation time, t_c, and the membrane shear elastic modulus, μ. The ensuing values, η = 0.38 to 0.88 μN/m·s, fall within the range of results reported from other independent experiments, 0.3 to 2.8 μN/m·s (29), for healthy RBCs. It is evident that both shear modulus and shear viscosity increase as a result of mechanical fatigue. The rate of fatigue-induced stiffening also increases with applied voltage. The shear viscosity increases from 0.72 μN/m·s at $N = 1$ to 2.93 μN/m·s at $N = 900$. This change can be represented by an exponential function $\eta = 0.68 \times \exp(1.7 \times 10^{-3} \times N)$ with $R^2 = 0.98$. Note that shear modulus and shear viscosity values measured after 900 cycles of fatigue loading at the highest load level of 2.0 V were as high as to 14.7 μN/m and 6.95 μN/m·s, respectively. These values are much higher than the corresponding upper-bound values reported for healthy, unfatigued (but statically or monotonically deformed) RBCs (29, 31). This trend again suggests that mechanical fatigue leads to alterations in structure and properties, including the stiffening of the cell membrane, of healthy RBCs that are distinctly different from those induced by static or monotonic loads.

Values of t_c are analyzed with an exponential fit to $\lambda(t)$ during the relaxation phase (such as that shown in the nonshaded region of Fig. 2*A*). *SI Appendix*, Fig. S3 shows the variation of t_c as a function of N, for 5 different voltage levels. For example, in the initial fatigue cycle for 1.0 V, $t_c = 0.16 \pm 0.04$ s, which is consistent with the values of 0.1 to 0.3 s reported in the literature on the basis of independent experimental techniques (31, 32). However, no correlation was found between t_c and the level of the applied voltages. After a sufficient number of cycles at 1.0 V, t_c increases to 0.17 ± 0.06 s, 0.21 ± 0.07 s, 0.22 ± 0.08 s, 0.28 ± 0.08 s, and 0.34 ± 0.10 s for N = 150, 300, 450, 600, and 900, respectively. Such progressive change in cellular relaxation behavior reflects the accumulation of viscous damage in RBC membranes as a result of mechanical fatigue.

In an attempt to quantify the stress dependence of fatigue damage in RBC membranes, we explore the conditions surrounding a 5% reduction in λ_{max} and define a critical number of fatigue cycles, N_s, required to achieve this level of change for different fatigue loading conditions. On the basis of this estimate, it is possible to develop a stress-life curve for the fatigue of RBCs, somewhat similar to the classical Wöhler curve in metal fatigue (1), which is shown in *SI Appendix*, Fig. S4.

Effect of Static Tensile Loading. In order to determine whether there exists a true mechanical fatigue effect in biological cells, we now consider static loading at a level of 1.2 V (Movie S2). The applied shear stress for this fixed load is estimated to be 2.85 Pa for the assumed membrane thickness of 10 nm. Fig. 3*A* shows the deformation response of 2 representative RBCs for which the relative stretch ratio S_R is plotted as a function of time over which the voltage (load) is applied for 60 min. Each cell is stretched to a maximum S_R in a finite time and the initial elastic stretch from the sudden application of load persists for at least 10 min. Afterward, the S_R value decreases with time, indicating the stiffening process in RBC membranes due to the cumulative deleterious effect from sustained loading. This finding agrees with a previous study (33) that showed reduced deformability arising from sustained mechanical loads. Differences in the cellular behavior between these 2 cells likely arise from the normal heterogeneity in cell membranes. A small fraction of RBCs (30%) exhibited tank-treading motion after a certain period of time, which could be a manifestation of structural alteration in cell membranes as noted previously (34). This phenomenon is demonstrated by the time-dependent oscillations in S_R values after ∼12 min in cell #2 (Fig. 3*A* and Movie S3). In order to quantify the progressive change in the mechanical properties in RBC membranes during static loading, the preset parameters μ, η, and ε_p have been obtained by a brief (20-s) deactivation of the static loading at every 10-min interval in a separate experiment but in parallel with the 60-min static loading. Fig. 3 *B*–*D* show the values of ε_p, μ, and η, respectively, averaged from 20 cells. Values of μ measured at $t = 20$ min are not significantly different from those measured at $t = 10$ min, while the values of η and ε_p are significantly higher ($P < 0.001$). All 3 parameters further increase during subsequent time intervals ($P < 0.001$). These results suggest, as anticipated, that static mechanical loading leads to changes in the characteristics of RBC membranes.

We develop additional quantitative comparisons of static deformation of RBCs with mechanical fatigue by contrasting the results for 2 different frequencies of constant-amplitude cyclic loading (rectangular waveform): 1) a time period of loading which occurs over 2 s, immediately followed by unloading lasting 2 s (i.e., a cyclic frequency of 0.25 Hz) for 2 applied voltages of 1.2 V and 2.0 V and 2) loading over 10 s, immediately followed by unloading lasting 10 s (i.e., a cyclic frequency of 0.05 Hz), also for the same 2 applied voltages of 1.2 V and 2.0 V. The deterioration in maximum deformation is quantified by the normalized relative extension

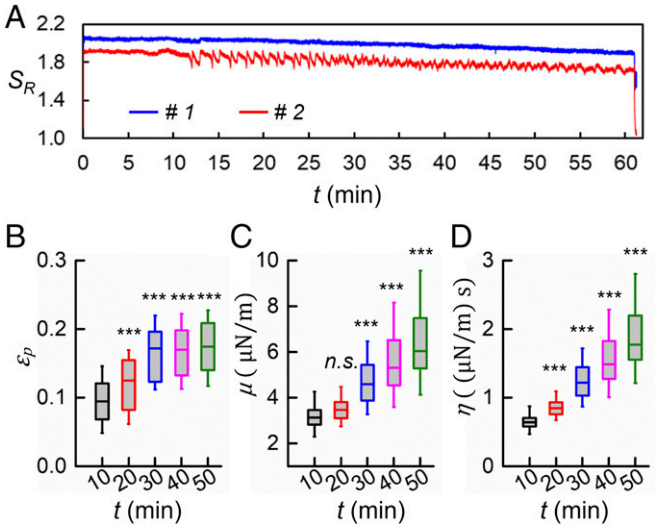

Fig. 3. Mechanical response of RBCs under static tensile loading. (*A*) Variation of relative stretch ratio as a function of time of 2 representative cells, #1 and #2, under the static loading at a constant voltage level of 1.2 V. (*B*–*D*) Values of ε_p, μ, and η of cells ($n = 20$) measured at 10, 20, 30, 40, and 50 min, respectively. ***$P < 0.001$; n.s., nonsignificant. Note the results here for static loading at the voltage of 1.2 V for 50 min correspond approximately to that obtained for cyclic loading with only 25 min of accumulated loading time at 1.2 V for 750 fatigue cycles (at a frequency of 0.25 Hz).

ratio, $\lambda^*_{max} = \lambda_{max}/\lambda_{max,t=0}$. This represents the ratio of the instantaneous value of the relative extension ratio, λ_{max}, of the RBC to that of the initial value of λ_{max} at time $t = 0$. Fig. 4 shows the changes in λ^*_{max} as a function of accumulated time under maximum load for static loading for the imposed voltages of 1.2 and 2 V in comparison to those under cyclic loading for the 2 frequencies with a rectangular waveform. This figure establishes that cyclic loading leads to a significantly greater reduction in the deformability of the cells than static loading. At the larger load, the lower-frequency cyclic loading (longer loading time) shows a relatively smaller loss in deformability (and a trend closer to that of the static loading case). The relative loss of deformability of RBCs under cyclic loading was as much as 11.9 ± 0.01% for 1.2 V and 21.7 ± 0.02% for 2 V, compared to the static loading case. The actual variation of λ_{max} as a function of time is shown in *SI Appendix*, Fig. S5.

Effect of Loading Waveform on Mechanical Fatigue. As strain rate is an important variable, along with strain, for the characterization of viscoelastic behavior of cell membranes (35, 36), we examined the effect of waveform (for a fixed cyclic loading frequency of 0.25 Hz). For this purpose, we compared mechanical fatigue with a rectangular waveform to that with a half-wave rectified (HWR) sinusoidal waveform. This latter waveform was achieved by modulating the amplitude of the 1.58-MHz carrier wave, $V = 1.2\sin(\pi t/2)$, with the period of 4 s, which comprised a 2-s duration of loading time (*SI Appendix*, Fig. S6*A* and Movie S4) and an equal time for unloading (with the voltage turned off) and relaxation. *SI Appendix*, Fig. S6*B* shows the instantaneous S_R values of RBC membranes, averaged from 22 measurements, as a function of time at fatigue loading cycles, $N = 1$, 300, 450, 600, and 900. We observed that cell membranes gradually deformed to a maximum S_R and then gradually relaxed to a minimum during each cycle. The 2-s relaxation interval was sufficient for deformed cell membranes to fully recover their shape before the next loading cycle.

Similar to the fatigue characteristics of cell membranes under rectangular-waveform cyclic loading, the maximum S_R values for the sinusoidal loading was found to decrease with the number of loading cycles while the minimum S_R increased along with the loading cycles (*SI Appendix*, Fig. S6*B*). The peaks of the S_R shifted and showed a greater hysteresis of membrane cyclic deformation with increasing fatigue cycles (marked by the dashed line in *SI Appendix*, Fig. S6*A*). The lag between the peak stress and peak deformation S_R increased approximately from 0 s at $N = 1$ to 0.13 s at $N = 900$, indicating an increase in viscosity of the cell membrane. To quantify the membrane viscosity, the characteristic time t_c was determined from the relaxation process when the external force was removed, using *SI Appendix*, Eq. **9** similarly to that used to obtain *SI Appendix*, Fig. S3. A significant rise in t_c was noticed, from 0.16 s to 0.43 s in ~900 loading cycles.

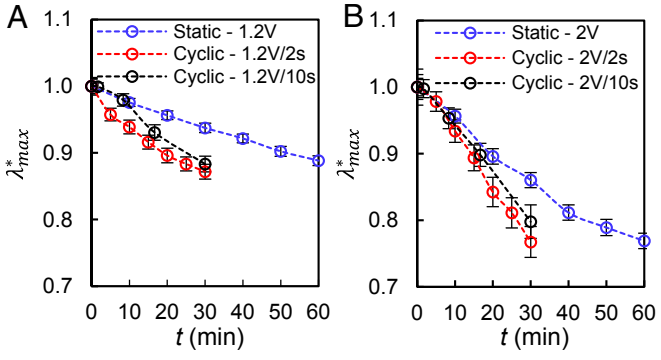

Fig. 4. Reduction of maximum relative deformation of RBCs as a function of accumulated loading time under static loading and cyclic loading with a rectangular waveform: Normalized λ^*_{max} of healthy cells under (*A*) 1.2 V static loading ($n = 35$, blue circles), 1. 2 V–2 s cyclic loading ($n = 58$, red circles), and 1. 2 V–10 s cyclic loading ($n = 49$, black circles) and (*B*) 2.0 V static loading ($n = 27$, blue circles), 2.0–2 s cyclic loading ($n = 20$, red circles), and 2.0 V–10 s cyclic loading ($n = 40$, black circles). Error bars indicate SEM. Similar results comparing maximum extension ratio along the axial direction of loading between static and cyclic loading cases are given in *SI Appendix*.

Fig. 5*A* shows the stress–strain (σ–ε) hysteresis loops of cell membranes. The maximum shear strain decreased gradually from 0.96 at $N = 1$ to 0.84, 0.74, 0.59, and 0.53 at $N = 300$, 450, 600, and 900, respectively. More importantly, we observed appreciable progressive change in the dissipated hysteresis energy E, determined from the enclosed area of the fatigue hysteresis loop. During the initial 300 loading cycles, the value of E remained approximately constant at 0.20 to 0.21 μJ/m^2 and then gradually increased to 0.31 μJ/m^2 for $N = 450$ before attaining a plateau value of ~0.40 μJ/m^2 between $N = 600$ and $N = 900$. Correlation between the dissipated energy E and the number of loading cycles was strong with $R^2 = 0.99$, with the best-fit Boltzmann growth line given by the expression $E = 0.4$ to $0.2/(1 + \exp((N - 445)/50))$ μJ/m^2. The total dissipated energy up to the inflection point ($N = 445$ cycles) was estimated to be 96 μJ/m^2, which is on the order of the energy, 80 μJ/m^2, required for dissociation between the phospholipid bilayer of the RBC membrane and its cytoskeletal comprising the spectrin network (15). The values of ε_p, μ, and η for the HWR sinusoidal waveform loading were compared to those for the rectangular waveform loading (Fig. 5 *B*–*D*). The membrane shear modulus is higher in the case of rectangular waveform loading than that for the sinusoidal amplitude loading. Here, the shear modulus for the former became significantly higher after 300 loading cycles ($P < 0.001$). However, η is not significantly different between the 2 different waveforms ($P > 0.05$ after 900 cycles). Furthermore, the evolution of permanent deformation, ε_p, in cell membranes was significantly faster for the rectangular waveform than for the sinusoidal waveform ($P < 0.05$ after 300 cycles).

Discussion and Concluding Remarks

In this work, we demonstrated a mechanical fatigue testing method for biological cells, using a microfluidics-based, amplitude-modulated, electrodeformation technique. The fatigue testing platform features multiple and unique advantages for the quantitative characterization of fatigue of single biological cells. The strengths of the method lie in its simplicity and flexibility to impose controlled mechanical loads (through positive DEP) at selected frequencies and waveforms, and its capability to probe a number of single cells over thousands of fatigue cycles. In this paper, we have presented results here that quantitatively establish the following results and mechanistic insights:

1) Repeated cyclic loading of healthy human RBCs under well-controlled loads, cyclic frequency, and waveform leads to an intrinsic mechanical fatigue effect in the biological cell. Our experimental method provides a unique means of quantifying cyclic deformation characteristics along and transverse to the loading direction (in *SI Appendix*, Figs. S8 and S9 and here in the main text) and their implications for the properties and performance of RBCs.

2) Mechanical fatigue of RBCs leads to a much more pronounced effect on the physical properties such as deformability, membrane shear modulus, and membrane viscosity than static loading of the same maximum voltage or load imposed on the cell for the same accumulated loading time.

3) Mechanical fatigue leads to hysteresis and energy dissipation of a magnitude that could be sufficient to cause dissociation of the cell membrane from its cytoskeleton, and that permanent strains progressively accumulate with fatigue cycling. These results illustrate how continued mechanical fatigue can be detrimental to the structural integrity, and hence the biological function, of the RBC, beyond the damage induced by static loads.

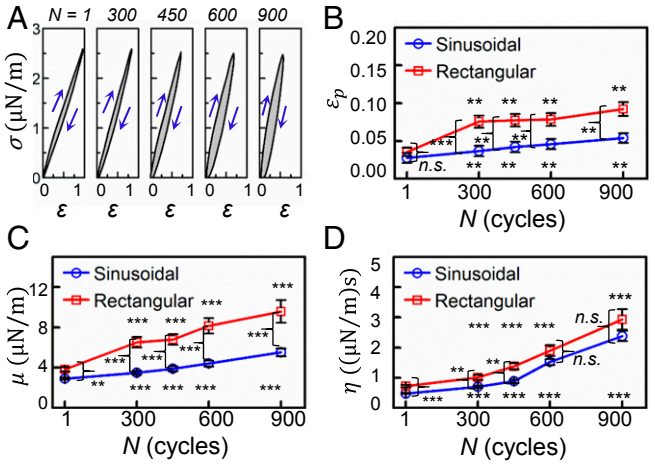

Fig. 5. Effect of loading waveform on mechanical degradation of RBCs during constant-amplitude mechanical fatigue. (*A*) Stress–strain curves showing the hysteresis loops (shaded region enclosed by the loading and unloading curves) for the indicated number of fatigue cycles for the HWR sinusoidal waveform. Blue arrows indicate loading and unloading in each case. (*B–D*) Variation of of ε_p, μ, and η as a function of the number of fatigue cycles, and comparisons of mechanical characteristics between the HWR sinusoidal loading and the rectangular step-function waveforms for the indicated fatigue cycles. Error bars indicate SEM. $^{**}P < 0.01$, $^{***}P < 0.001$; n.s., nonsignificant.

4) The values of membrane shear modulus, viscosity, and the characteristic time of relaxation extracted from our experiments at the commencement of fatigue loading are in the range of values reported in the literature for healthy, unfatigued RBCs, using a variety of independent experimental methods. We show systematically that with the progression of mechanical fatigue the membrane shear modulus increases, approaching values that are comparable to pathological RBCs structurally altered by disease states. For example, the increase in membrane shear modulus of the healthy RBC to about 15 μN/m solely as a result of mechanical fatigue within 1,000 fatigue cycles is roughly comparable in magnitude to the increase in membrane shear modulus of a ring-stage RBC after it is invaded by a *Plasmodium falciparum* malaria parasite (20, 27).

The conditions of fatigue loading in our in vitro microfluidic assay are constrained by the need to allow cells to fully relax from the deformed state after each fatigue cycle prior to the imposition of the next cycle. This somewhat limited the choice of the loading frequency. To ascertain that the cells were viable through the entire duration of the mechanical fatigue tests, we conducted a series of separate experiments to determine the viability of RBCs after 1 h of cyclic loading at 1.2 V at a frequency of 0.25 Hz with rectangular waveform. Standard cell viability assays (for details see *SI Appendix, RBC Viability Assay*) reveal that about 98% of the cells are still viable after mechanical fatigue testing.

Additional considerations of how the current in vitro results of mechanical fatigue connect to the much more complex in vivo conditions of cyclic straining are provided herein. The maximum (absolute) tensile strain within the RBC membrane (spectrin network) while the RBCs traverse the smallest capillaries was estimated to be on the order of 50% (corresponding to a local spectrin network stretch ratio of 1.7) (37). Note that these maximum tensile strain values are comparable to the average tensile strains obtained by optical tweezers experiments of healthy RBCs stretched uniaxially under a tensile force of 67 to 130 pN (38, 39). The extent of deformation induced by the electric field on the RBCs in our work is also comparable to the mechanical deformation imposed by optical tweezers under equivalent stretching forces (40). When RBCs circulate in larger blood vessels, they experience much less distortion and deformation. Considering that the maximum strain due to bending and total bending energy are both relatively much smaller compared to the in-plane strains and related strain energy due to stretch or shear [in most cases influences from bending are negligible compared to stretch (41, 42)], we take the zero strain as the minimum RBC membrane strain during blood circulation.

Considering that the lung-to-lung circulation time of blood in healthy subjects is about 55 s (43), and that the average lifespan of a healthy RBC in the human body is about 120 d, we can estimate the total number of fatigue cycles that an RBC is subjected to is about 1.9×10^5. This estimate of in vivo fatigue cycles is about 200 times greater than the maximum number of fatigue cycles of about 900 considered in our in vitro system, during the course of which significant fatigue damage is found to occur.

Such a comparison then raises the following question: How do RBCs perform their biological function of gas transport in vivo without being affected by the effects of mechanical fatigue that can occur in as few as 900 cycles (i.e., about 0.5% of their lifespan)? This apparent paradox is rationalized on the basis of the following considerations. First, the maximum DEP electric field in our experiments would load RBCs in such a way that it produces an average tensile strain similar to the maximum local strains RBCs experience when traversing the smallest capillaries. In other words, our testing conditions simulate beyond the most stringent mechanical constraint conditions in vivo that lead to the maximum local strains, and they do not simulate the typical average cyclic strain on the RBCs during their lifespan. In addition, in our experiments the RBCs are quickly shuffled between the 2 extreme situations (maximum tension and zero strain), while in vivo the RBCs take an average of about 55 s between the maximum mechanical challenge and many partially unloaded intermediate configurations. Second, there are many additional factors that contribute to the fatigue life of RBCs, including the type of deformation, stress/strain amplitudes, cyclic frequency, loading rate, cytoadherence between their external surfaces and the endothelial cells lining the blood vessels, and so on. These effects representing complex in vivo conditions are not fully captured in the in vitro experiments. Third, in our experiments we find that RBCs do not lyse even after 900 cycles simulating severe deformation conditions. It is likely that significantly greater numbers of mechanical fatigue are needed to lyse the RBCs.

As in our in vitro testing, RBCs are subjected to rigorously modulated loading conditions, including static and cyclic deformation at various stress levels. Our method thus provides an accelerated test for assessing fatigue failure in RBC membranes due to mechanical loading.

On the other hand, as assessed by the viability assay of RBCs subjected to 1 h (900 cycles) of loading, the viability of RBCs is very high, at 98 ± 2% (see the discussion on RBC viability in *SI Appendix, RBC Viability Assay*). Therefore, it is likely that the electric field does not contribute significantly to the difference between the in vivo and in vitro observations.

The system developed here is also amenable to conducting mechanical fatigue experiments in conjunction with cellular gaseous microenvironments (44, 45) to create realistic, multifaceted loading scenarios to relate in vitro fatigue characteristics to the in vivo behavior of RBCs subjected to repeated straining during blood circulation. A recently developed hypoxia assay for the study of sickle cell disease (45, 46) in a microfluidic system can be integrated into the current fatigue testing platform to measure the mechanical strength and residual life span of circulating RBCs in more physiologically appropriate conditions.

Methods

Experimental Setup. The microfluidic chips for the fatigue test were made using a polydimethylsiloxane channel with 2 interdigitated electrodes coated on glass. More details are given in *SI Appendix, Experimental Setup*.

Sample Preparation. Blood samples from healthy donors were obtained with institutional review board approval from Florida Atlantic University. All blood samples used were deidentified prior to use in the study. More details are given in *SI Appendix, Sample Preparation*.

ACKNOWLEDGMENTS. This work was supported by National Science Foundation Grants 1635312 and 1464102. M.D. acknowledges support from NIH Grant U01HL114476. S.S. acknowledges Nanyang Technological University, Singapore, for support through the Distinguished University Professorship.

1. S. Suresh, *Fatigue of Materials* (Cambridge University Press, Cambridge, UK, ed. 2, 1998).
2. International ASTM, *Fatigue Standards and Fracture Standards* (International ASTM, West Conshohocken, PA, 2018).
3. L. B. Freund, S. Suresh, *Thin Film Materials: Stress, Defect Formation and Surface Evolution* (Cambridge University Press, Cambridge, UK, 2004).
4. J. J. Kruzic, R. O. Ritchie, Fatigue of mineralized tissues: Cortical bone and dentin. *J. Mech. Behav. Biomed. Mater.* **1**, 3–17 (2008).
5. K. Shemtov-Yona, D. Rittel, Fatigue of dental implants: Facts and fallacies. *Dent J (Basel)* **4**, E16 (2016).
6. R. H. Dauskardt, R. O. Ritchie, J. K. Takemoto, A. M. Brendzel, Cyclic fatigue and fracture in pyrolytic carbon-coated graphite mechanical heart-valve prostheses: Role of small cracks in life prediction. *J. Biomed. Mater. Res.* **28**, 791–804 (1994).
7. R. Bai, J. Yang, Z. Suo, Fatigue of hydrogels. *Eur. J. Mech. A Solid.* **74**, 337–370 (2019).
8. L. Musumeci *et al*., Prosthetic aortic valves: Challenges and solutions. *Front. Cardiovasc. Med.* **5**, 46 (2018).
9. S. Sakuma *et al*., Red blood cell fatigue evaluation based on the close-encountering point between extensibility and recoverability. *Lab Chip* **14**, 1135–1141 (2014).
10. M. J. Simmonds, H. J. Meiselman, Prediction of the level and duration of shear stress exposure that induces subhemolytic damage to erythrocytes. *Biorheology* **53**, 237–249 (2016).
11. T. Mizuno *et al*., Ultrastructural alterations in red blood cell membranes exposed to shear stress. *ASAIO J.* **48**, 668–670 (2002).
12. G. Bao, S. Suresh, Cell and molecular mechanics of biological materials. *Nat. Mater.* **2**, 715–725 (2003).
13. S. Suresh, Biomechanics and biophysics of cancer cells. *Acta Biomater.* **3**, 413–438 (2007).
14. J.-B. Fournier, D. Lacoste, E. Raphaël, Fluctuation spectrum of fluid membranes coupled to an elastic meshwork: Jump of the effective surface tension at the mesh size. *Phys. Rev. Lett.* **92**, 018102 (2004).
15. Z. Peng *et al*., Lipid bilayer and cytoskeletal interactions in a red blood cell. *Proc. Natl. Acad. Sci. U.S.A.* **110**, 13356–13361 (2013).
16. I. V. Pivkin *et al*., Biomechanics of red blood cells in human spleen and consequences for physiology and disease. *Proc. Natl. Acad. Sci. U.S.A.* **113**, 7804–7809 (2016).
17. C. E. Riva, J. E. Grunwald, S. H. Sinclair, B. L. Petrig, Blood velocity and volumetric flow rate in human retinal vessels. *Invest. Ophthalmol. Vis. Sci.* **26**, 1124–1132 (1985).
18. F. Lang, E. Lang, M. Föller, Physiology and pathophysiology of eryptosis. *Transfus. Med. Hemother.* **39**, 308–314 (2012).
19. A. M. Dondorp, P. A. Kager, J. Vreeken, N. J. White, Abnormal blood flow and red blood cell deformability in severe malaria. *Parasitol. Today* **16**, 228–232 (2000).
20. S. Suresh *et al*., Connections between single-cell biomechanics and human disease states: Gastrointestinal cancer and malaria. *Acta Biomater.* **1**, 15–30 (2005).
21. J. Narla, N. Mohandas, Red cell membrane disorders. *Int. J. Lab. Hematol.* **39** (suppl. 1), 47–52 (2017).
22. Y. Qiang, J. Liu, E. Du, Dynamic fatigue measurement of human erythrocytes using dielectrophoresis. *Acta Biomater.* **57**, 352–362 (2017).
23. Y. Qiang, J. Liu, F. Yang, D. Dieujuste, E. Du, Modeling erythrocyte electrodeformation in response to amplitude modulated electric waveforms. *Sci. Rep.* **8**, 10224 (2018).
24. E. H. Serpersu, K. Kinosita, Jr, T. Y. Tsong, Reversible and irreversible modification of erythrocyte membrane permeability by electric field. *Biochim. Biophys. Acta* **812**, 779–785 (1985).
25. L. B. Leverett, J. D. Hellums, C. P. Alfrey, E. C. Lynch, Red blood cell damage by shear stress. *Biophys. J.* **12**, 257–273 (1972).
26. Y. Qiang, J. Liu, E. Du, Dielectrophoresis testing of nonlinear viscoelastic behaviors of human red blood cells. *Micromachines (Basel)* **9**, 21 (2018).
27. J. P. Mills *et al*., Effect of plasmodial RESA protein on deformability of human red blood cells harboring Plasmodium falciparum. *Proc. Natl. Acad. Sci. U.S.A.* **104**, 9213–9217 (2007).
28. H. Zhang, K.-K. Liu, Optical tweezers for single cells. *J. R. Soc. Interface* **5**, 671–690 (2008).
29. R. M. Hochmuth, R. E. Waugh, Erythrocyte membrane elasticity and viscosity. *Annu. Rev. Physiol.* **49**, 209–219 (1987).
30. M. M. Haque, M. G. Moisescu, S. Valkai, A. Dér, T. Savopol, Stretching of red blood cells using an electro-optics trap. *Biomed. Opt. Express* **6**, 118–123 (2014).
31. S. Chien, K. L. Sung, R. Skalak, S. Usami, A. Tözeren, Theoretical and experimental studies on viscoelastic properties of erythrocyte membrane. *Biophys. J.* **24**, 463–487 (1978).
32. R. M. Hochmuth, P. R. Worthy, E. A. Evans, Red cell extensional recovery and the determination of membrane viscosity. *Biophys. J.* **26**, 101–114 (1979).
33. M. Horade, C.-H. D. Tsai, H. Ito, M. Kaneko, Red blood cell responses during a long-standing load in a microfluidic constriction. *Micromachines* **8**, 100 (2017).
34. T. M. Fischer, M. Stöhr-Lissen, H. Schmid-Schönbein, The red cell as a fluid droplet: Tank tread-like motion of the human erythrocyte membrane in shear flow. *Science* **202**, 894–896 (1978).
35. Y.-Z. Yoon, J. Kotar, G. Yoon, P. Cicuta, The nonlinear mechanical response of the red blood cell. *Phys. Biol.* **5**, 036007 (2008).
36. J. Mancuso, W. Ristenpart, Stretching of red blood cells at high strain rates. *Phys. Rev. Fluids* **2**, 101101 (2017).
37. D. J. Quinn *et al*., Combined simulation and experimental study of large deformation of red blood cells in microfluidic systems. *Ann. Biomed. Eng.* **39**, 1041–1050 (2011).
38. M. Dao, C. T. Lim, S. Suresh, Mechanics of the human red blood cell deformed by optical tweezers. *J. Mech. Phys. Solids* **51**, 2259–2280 (2003).
39. J. P. Mills, L. Qie, M. Dao, C. T. Lim, S. Suresh, Nonlinear elastic and viscoelastic deformation of the human red blood cell with optical tweezers. *Mech. Chem. Biosyst.* **1**, 169–180 (2004).
40. E. Du, M. Dao, S. Suresh, Quantitative biomechanics of healthy and diseased human red blood cells using dielectrophoresis in a microfluidic system. *Extreme Mech. Lett.* **1**, 35–41 (2014).
41. Y. C. Fung, P. Tong, Theory of the sphering of red blood cells. *Biophys. J.* **8**, 175–198 (1968).
42. R. Skalak, A. Tozeren, R. P. Zarda, S. Chien, Strain energy function of red blood cell membranes. *Biophys. J.* **13**, 245–264 (1973).
43. N. R. Morris, E. M. Snyder, K. C. Beck, B. D. Johnson, Lung-to-lung circulation times during exercise in heart failure. *Eur. J. Appl. Physiol.* **106**, 621–627 (2009).
44. F. Padilla, P. A. Bromberg, W. N. Jensen, The sickle-unsickle cycle: A cause of cell fragmentation leading to permanently deformed cells. *Blood* **41**, 653–660 (1973).
45. E. Du, M. Diez-Silva, G. J. Kato, M. Dao, S. Suresh, Kinetics of sickle cell biorheology and implications for painful vasoocclusive crisis. *Proc. Natl. Acad. Sci. U.S.A.* **112**, 1422–1427 (2015).
46. E. Du, M. Dao, Faster sickling kinetics and sickle cell shape evolution during repeated deoxygenation and oxygenation cycles. *Exp. Mech.* **59**, 319–325 (2019).

PNAS
www.pnas.org

Supplementary Information for

Mechanical fatigue of human red blood cells

Yuhao Qiang, Jia Liu, Ming Dao*, Subra Suresh*, E Du*

*Ming Dao, E-mail: mingdao@mit.edu
*Subra Suresh, E-mail: ssuresh@ntu.edu.sg
*E Du, E-mail: edu@fau.edu

This PDF file includes:

Supplementary text
Figs. S1 to S9
Table S1
Captions for Movies S1 to S4
References for SI reference citations

Other supplementary materials for this manuscript include the following:

Movies S1 to S4

Supplementary Information

Experimental Setup. The microfluidic chip designed for conducting the fatigue test consists of a 50 μm deep, 500 μm wide and 10 mm long polydimethylsiloxane (PDMS) microfluidic channel and two interdigitated electrodes (with 20 μm gap and 20 μm band width) coated on 0.7 mm thick glass. The electrical excitation system consists of a printed circuit board (PCB) with a microscopic observation area and a signal generator (SIGLENT SDG830, SIGLENT, P.R. China). Red blood cell (RBC) deformation was observed through a high-resolution CMOS camera (The Imaging Source, Charlotte, NC) which is mounted on an Olympus X81 inverted microscope (Olympus America, PA, USA), where image contrast was enhanced by inserting a 414 ± 46 nm band pass filter in the optical path. The microfluidic channel was coated with dielectrophoresis (DEP) buffer solution with 5% bovine serum albumin (BSA, Lot 20150520AS, Rocky Mountain Biologicals. Inc, Missoula, MT) for more than 30 min before each test, so as to prevent adhesion of the cell to the bottom of the channel. Any excess coating medium in the channel was then removed along with the DEP buffer before the cell suspension was injected into the microfluidic chip.

Sample Preparation. Blood samples from healthy donors were obtained with institutional review board (IRB) approval from Florida Atlantic University. All blood samples used were de-identified prior to use in the study. The DEP buffer was prepared by mixing 8.5% (w/v) sucrose and 0.3% (w/v) dextrose in deionized water, and further adjusting electrical conductivity to 0.02 S/m using phosphate buffered saline (PBS) solution (Lonza Walkersville, Inc., Walkersville, MD). Prior to each fatigue test, blood samples were gently washed twice with PBS at 2,000 rpm for 2 min at room temperature. The RBC pellet was collected and re-suspended in the DEP buffer to a final concentration of 10^6 cells/ml.

Statistical Study. RBCs were individually tracked as a function of time during the course of the experiments. Statistical analyses were performed using OriginPro 9 (OriginLab, Northampton, MA). All data were expressed in terms of statistical mean ± SD, except stated otherwise. A paired *t*-test between measurements of samples from the initial cycle and subsequent cycles was used to generate *p* values. A two-sample *t*-test was used to generate the *p* values between measurements for different loading cases. The *p* values equal to or smaller than 0.05 were considered statistically significant differences between the results that were compared. For correlation studies, R^2 (the *R*-squared values) are listed.

Electro-deformation Characterization of RBCs

As a result of interfacial Maxwell–Wagner polarization across the cellular membrane (1), the RBC is subjected to a DEP force from the dipole moment induced by a non-uniform electric field. The direction and magnitude of the DEP force depend on the electrical properties of the cell and the surrounding medium as well as the on the amplitude and frequency of the electric field. Assuming that the shape of RBC can be approximated as an ellipsoid, the time-averaged DEP force can be quantified by (1)

$$\langle F_{\mathrm{DEP}} \rangle = \frac{\pi}{4} abc \cdot \epsilon_{\mathrm{m}} \cdot Re(f_{\mathrm{CM}}) \cdot \nabla E_{\mathrm{rms}}^2 \tag{1}$$

where *a*, *b* and *c* are the dimensions along *x*, *y* and *z* axes of the RBC, respectively; ϵ_{m} is the permittivity of the surrounding medium, and ∇E_{rms} the root-mean-square of the gradient of electric field strength. The direction of electro-deformation force exerted on the RBC is determined by the value of the real part of the Clausius Mossotti factor (f_{CM}), $Re(f_{\mathrm{CM}})$. When $Re(f_{\mathrm{CM}})$ is positive, the cells move toward the electrode, and eventually get trapped at the electrode edges under positive electro-deformation. Conversely, under negative DEP ($Re(f_{\mathrm{CM}}) < 0$), the cells are repelled from the electrodes. The value of f_{CM} can be estimated using a concentric multi-shell model (2, 3),

$$f_{\mathrm{CM}} = \frac{1}{3} \frac{(\epsilon_{\mathrm{mem}}^* - \epsilon_{\mathrm{m}}^*)[\epsilon_{\mathrm{mem}}^* + A_1(\epsilon_{\mathrm{cyto}}^* - \epsilon_{\mathrm{mem}}^*)] + \rho(\epsilon_{\mathrm{cyto}}^* - \epsilon_{\mathrm{mem}}^*)[\epsilon_{\mathrm{mem}}^* - A_1(\epsilon_{\mathrm{mem}}^* - \epsilon_{\mathrm{m}}^*)]}{(\epsilon_{\mathrm{m}}^* + A_1(\epsilon_{\mathrm{mem}}^* - \epsilon_{\mathrm{m}}^*))\left[\epsilon_{\mathrm{mem}}^* + A_1(\epsilon_{\mathrm{cyto}}^* - \epsilon_{\mathrm{mem}}^*)\right] + \rho A_2(1 - A_2)(\epsilon_{\mathrm{cyto}}^* - \epsilon_{\mathrm{mem}}^*)(\epsilon_{\mathrm{mem}}^* - \epsilon_{\mathrm{m}}^*)} \tag{2}$$

where the subscripts mem, m and cyto represent membrane, medium and cytoplasm, respectively. $\epsilon^* = \epsilon - \mathrm{j}\delta/\omega$, where ω, ϵ and δ are the angular frequency, dielectric permittivity and conductivity, respectively. $\rho = (a-d)(b-d)(c-d)/(abc)$, where *d* denotes the thickness of the cell membrane. $A_{i=1,2}$ is the depolarization factor, defined as

$$A_i = \frac{a_i b_i c_i}{2} \int_0^\infty \frac{ds}{(s+a_i^2)B_i}, i = 1, 2 \quad (3)$$

where s is a dummy integration variable, $B_i = \sqrt{\left((s+a_i^2)(s+b_i^2)(s+c_i^2)\right)}$, $a_1 = a$, $b_1 = b$, $c_1 = c$, $a_2 = a - d$, $b_2 = b - d$, and $c_2 = c - d$.

Table S1. Typical values of parameters used in the calculation of $Re(f_{CM})$ of healthy RBCs(4, 5)

Cell	*a* (μm)	*b* (μm)	*c* (μm) (4)	*d* (nm) (5)	ϵ_{mem} (5)	δ_{mem} (S/m) (5)	ϵ_{cyto} (5)	δ_{cyto} (S/m) (5)	ϵ_{m}	δ_{m} (S/m)
Healthy RBCs	8	8	2.6	4.5	4.44	10^{-6}	59	0.31	80	0.02

As shown in Fig. S1A, $Re(f_{\text{CM}})$ was calculated as a function of the electrical frequency using Eq. (2) based on the geometrical parameters and properties of healthy RBCs, which are available from the literature (4, 5) (Table S1). For the chosen frequency of 1.58 MHz in our experiment, electrical excitation provides a favorable positive DEP effect on RBCs. To evaluate the influence of possible variations in DEP on RBCs, we performed parametric analysis of $Re(f_{\text{CM}})$ by multiplying the electrical properties of subcellular components in Table S1 with a factor, k. $Re(f_{\text{CM}})$ decreased from 1.252 to only 1.247 as k increased from unity to 2 for membrane conductivity, δ_{mem} (Fig. S1B). The value of $Re(f_{\text{CM}})$ slightly decreased from 1.253 to 1.249 when k ranged from 0.5 to 2 for cytoplasm permittivity, ϵ_{cyto} (Fig. S1C). These results show that $Re(f_{\text{CM}})$ is not sensitive to δ_{mem} and ϵ_{cyto}. It should also be noted that the value of $Re(f_{\text{CM}})$ increased from 0.96 to 1.44, as k ranged from 0.5 to 2 for cytoplasm conductivity, δ_{cyto} (Fig. S1D). Assuming a linear variation between the hemoglobin concentration and cytoplasmic conductivity, we find that $Re(f_{\text{CM}})$ is also not very sensitive to cytoplasmic conductivity.

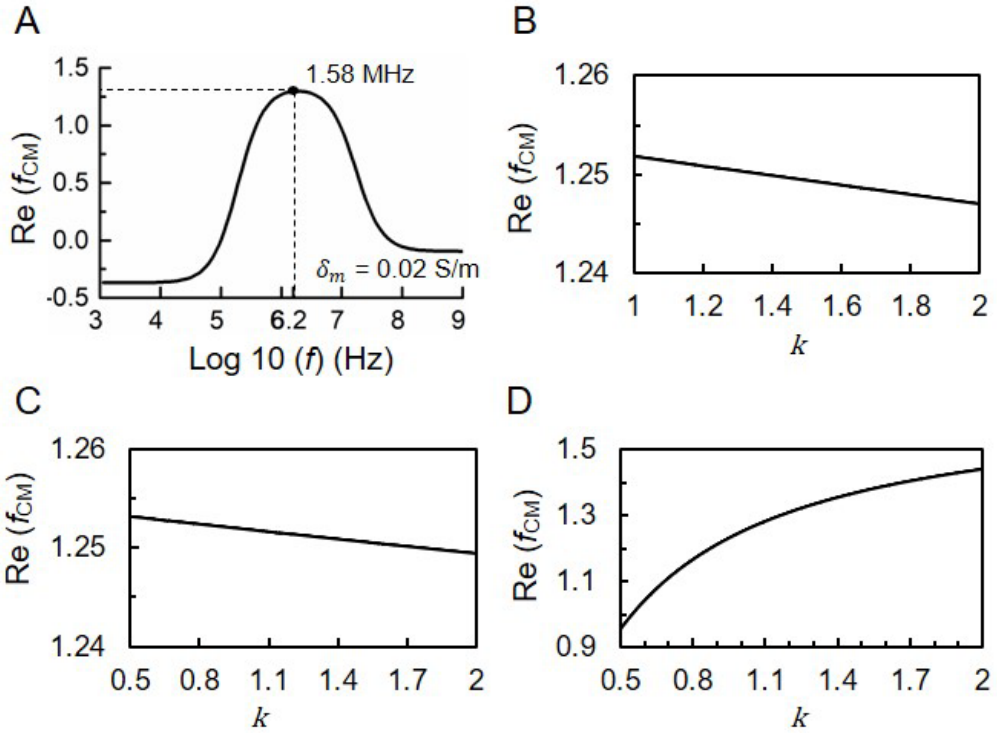

Fig. S1. Parametric analysis of DEP behavior of RBCs: (A) $Re(f_{\text{CM}})$ of healthy RBCs as a function of electrical frequency in the working medium with conductivity of 0.02 S/m. (B-D) $Re(f_{\text{CM}})$ of RBCs as functions of factor k for membrane conductivity, cytoplasm permittivity, and cytoplasm conductivity, respectively.

The Maxwell stress tensor (MST) method was used to calculate the electro-deformation force using the finite element analysis package COMSOL Multiphysics (Burlington, MA, USA). Here, the effects of cells on the distribution of electrical field was taken into account since cells have a size comparable to that of the electrodes and move toward the electrodes under positive DEP. The time-averaged tensor is given by (6)

$$\langle \boldsymbol{\sigma}^{\mathrm{MST}} \rangle = \frac{1}{4} Re[\tilde{\epsilon}](\boldsymbol{E}\boldsymbol{E}' + \boldsymbol{E}'\boldsymbol{E} - |\boldsymbol{E}|^2 \boldsymbol{I}) \tag{4}$$

$$\langle \boldsymbol{F} \rangle = \oint_S \langle \boldsymbol{\sigma}^{\mathrm{MST}} \rangle \cdot \boldsymbol{n} dS \tag{5}$$

where $\tilde{\epsilon}$ denotes the complex electrical permittivity, $\boldsymbol{E}$ the electrical field, $\boldsymbol{I}$ the unit second-order tensor, and the product of two vectors results in the dyadic product. S is the outer surface area of the cell, and $\boldsymbol{n}$ is the unit vector normal to the cell surface.

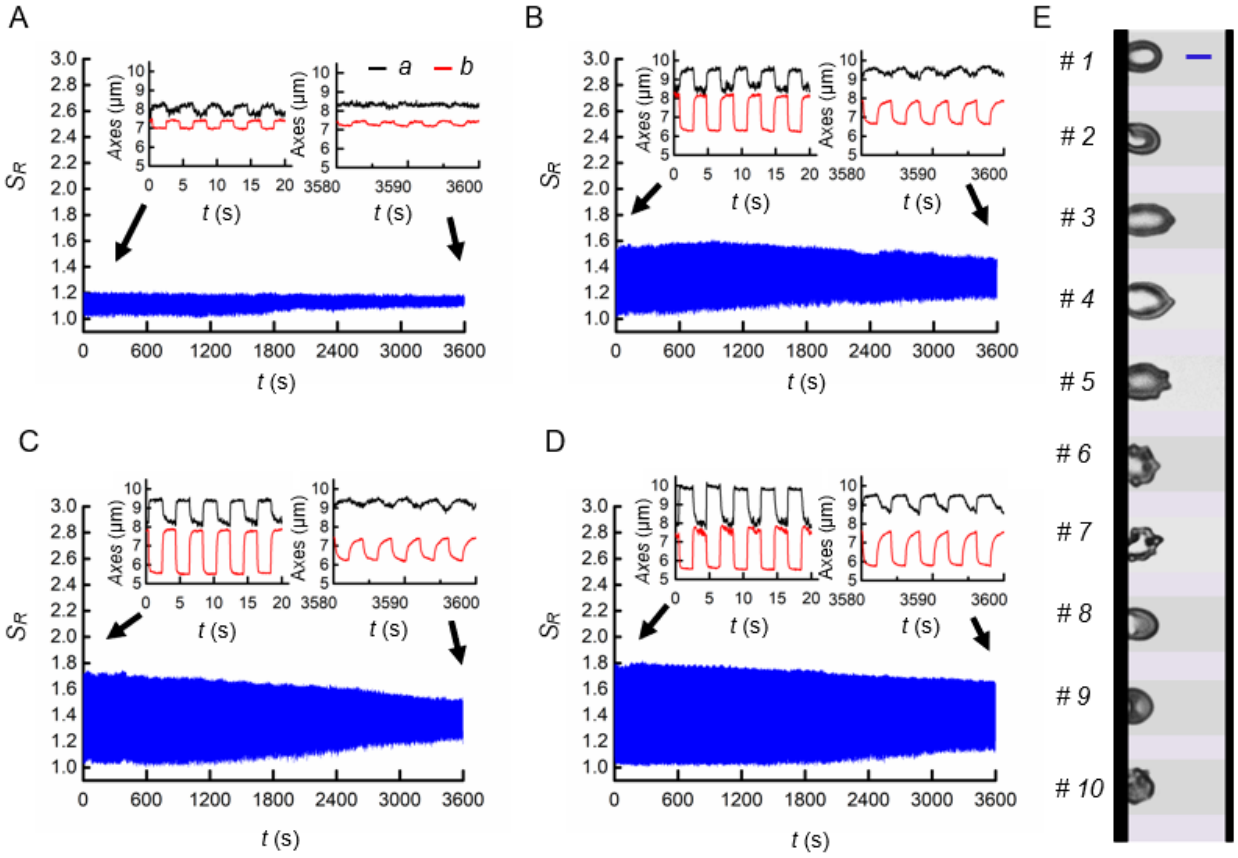

Fig. S2. Fatigue characteristics of RBCs in response to cyclic tensile loading with rectangular waveform for load ratio, R = 0 at variable voltage levels. (A-D) Quantitative measurements of the stretch ratio, S_R, as a function of time, for different representative cells in response to 0.5 V, 0.8 V, 1.0 V and 1.2 V, respectively. Insets indicate major and minor axes, *a* and *b* of ellipse-fitted cell shapes during the initial five and last five cycles (left and right insets, respectively). (E) Formation of permanent damage in cell membrane during cyclic loading: Cell # 1 after N = 855 at a peak load of 0.8 V, Cell # 2 after N = 250 at 1.0 V, Cell # 3 after N = 330 at 1 V, Cell # 4 after N = 185 at 2.0 V, Cell # 5 after N = 533 at 0.8 V, Cell # 6 after N = 100 at 1.5 V, Cell # 7 after N = 900 at 2.0 V, Cell # 8 after N = 360 at 1.5 V, Cell # 9 after N = 868 at 2.0 V, and Cell # 10 after N = 834 at 1 V. (Scale bars in E denote a length scale of 5 μm).

The evolution of the stretch ratios, S_R, from cyclic electro-deformation for four representative RBCs at different voltages of 0.5 V, 0.8 V, 1.0 V, and 1.2 V are plotted against time in Fig.S2*A*–*D*, respectively. In response to cyclic tensile loading, S_R values of cell membranes exhibit in-phase cyclic deformation patterns that are enveloped by upper and lower bound values. The envelope of maximal S_R represents the maximum deformation during each cycle and descends gradually with fatigue cycles; the bound of minimum S_R represents the fully relaxed cell membranes and its value increases gradually with fatigue cycles. The two bounds tend to approach each other, indicating the gradual hardening process and irreversible deformation in cell membranes with the progression of fatigue. The differences between the two bounds increase with the amplitude of the applied voltage. The insets in each plot in Fig. S2 indicate variations in the values of major and minor axes (*a* and *b,* respectively) of the RBC during the first five and last five cycles, for each of the four cell examples.

Constitutive Model for Viscoelastic Deformation of RBC Membranes

In response to shear stresses induced by the application of an electrical voltage, the RBC membrane exhibits viscoelastic deformation. Such behavior has been idealized using a time-dependent constitutive behavior described by the Kelvin-Voigt solid model (7, 8). For instance, under constant-amplitude cyclic electro-deformation loading, RBC membranes undergo viscoelastic behavior during each cycle of tensile-stretching and relaxation.

The transient extension ratio $\lambda(\mathrm{t})$ is defined as the ratio of the initial value of minor axis b_0 of the ellipse representing the shape of the RBC to the instantaneous value of the minor axis $b(t)$ at any time t in both the stretching and relaxation phases of fatigue. Note that $\lambda(t)$ is defined as $b_0/b(t)$ and not in terms of the longer-axis extension ratio, $a(t)/a_0$, because a small part of deformed membrane along the major axis, *a,* is necessarily obstructed from view by the gold electrode when imaging the cell, and this could lead to an error in the calculation if the latter definition of $\lambda(\mathrm{t})$ had been invoked. In a later section of this *SI Appendix*, we demonstrate that the definition of the instantaneous values extension ratio based either on the axial stretch, $a(t)/a_0$, or the corresponding transverse contraction, $b_0/b(t)$, has no effect on the trends discovered here about the role of mechanical fatigue in influencing the behavior of RBCs. The actual values of $\lambda(t)$ vary as anticipated because of the normal variations in cell response and experimental scatter in extracting axial and transverse dimensions during deformation from optical images.

The resulting shear strain ε is calculated as

$$\varepsilon(t) = \frac{(\lambda(t)^2 - \lambda(t)^{-2})}{2} \tag{6}$$

Specifically, transient shear stress σ from electro-deformation loading is determined by

$$\sigma(t) = \frac{F(t)}{2b(t)} \tag{7}$$

Thus, transient stress versus deformation relationship of single RBCs can be written according to the Kelvin-Voigt solid model, by combining Eqs. (6) and (7), as

$$\frac{\sigma(t)}{2\mu} = \frac{1}{4}(\lambda(t)^2 - \lambda(t)^{-2}) + t_c \frac{\partial \ln \lambda(t)}{\partial t} \tag{8}$$

where μ is the membrane shear modulus, $t_c \equiv \eta/\mu$ is the characteristic time for relaxation which is a material time constant, and η is shear viscosity. Value of t_c can be extracted from an exponential fit of the data of $\lambda(t)$ during the relaxation phase (when $\sigma = 0$),

$$\exp\left(-\frac{t}{t_c}\right) = \frac{(\lambda - \lambda_0)(\lambda_{\max} + \lambda_0)}{(\lambda + \lambda_0)(\lambda_{\max} - \lambda_0)} \tag{9}$$

where $\lambda_{\max}$ and λ_0 represent the values of λ measured in the fully-stretched and fully-relaxed states, respectively.

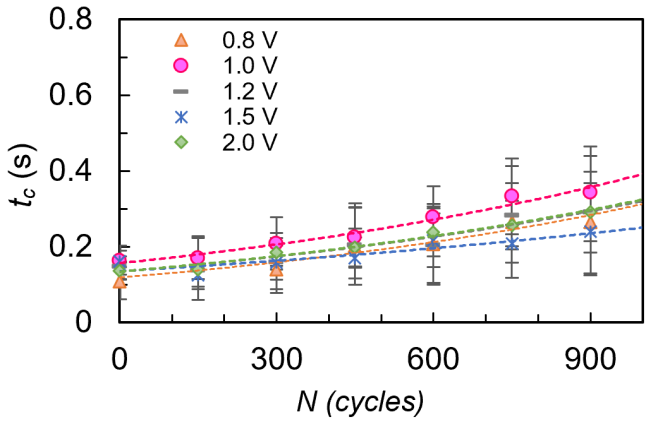

Fig. S3. The characteristic time of relaxation, t_c, of healthy RBCs for five different voltage levels, *V*, are plotted. The symbols denote experimental results of relaxation time calculated using Eq. (9). The dashed lines present the fit using an exponential function for each value of the voltage applied to the cells.

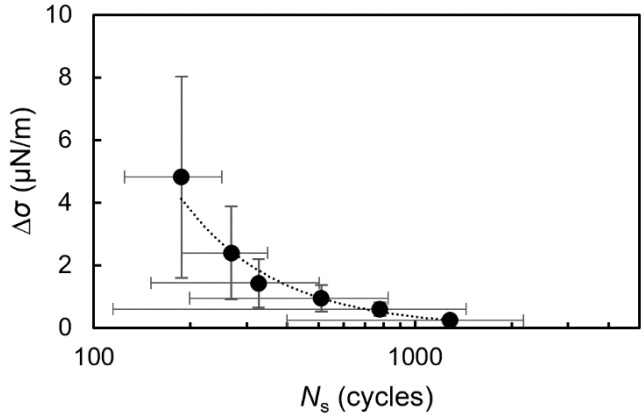

Fig. S4. The *S-N* diagram obtained from the fatigue testing of RBCs (*n* = 20). Here the number of cycles to life, N_s, is defined as that leading to a 5% reduction in λ_{max} as a result of cyclic loading and accumulated damage. The dashed curve represents the best fitting function to the Wöhler equation, $\Delta\sigma = 9184.2 \times (N_s)^{-1.473}$. Best fitting function for the Wöhler equation, $\Delta\sigma = \sigma_f \times (N_s)^b$ for the *S-N* data provides the strength factor, $\sigma_f = 9184\ \mu\mathrm{N/m}$, and the Basquin exponent, $b = -1.743$.

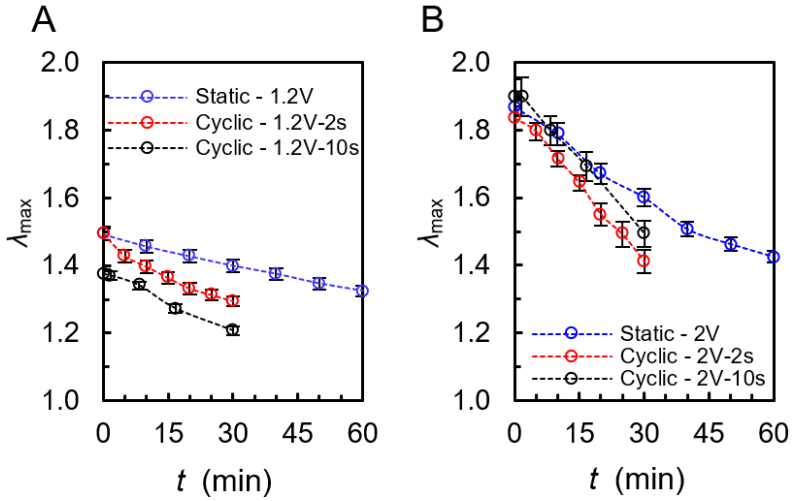

Fig. S5. Reduction of maximum deformation of cells as a function of accumulated loading time under static loading and cyclic loading: (A) Applied voltage of 1.2 V static loading (*n* = 35, blue circles), 1. 2 V–2 s cyclic loading (*n* = 58, red circles), and 1. 2 V–10 s cyclic loading (*n* = 49, black circles) (B) 2.0 V static loading (*n* = 27, blue circles), 2 V–2 s cyclic loading (*n* = 20, red circles), and 2 V–10 s cyclic loading (*n* = 40, black circles). Error bars indicate SEM.

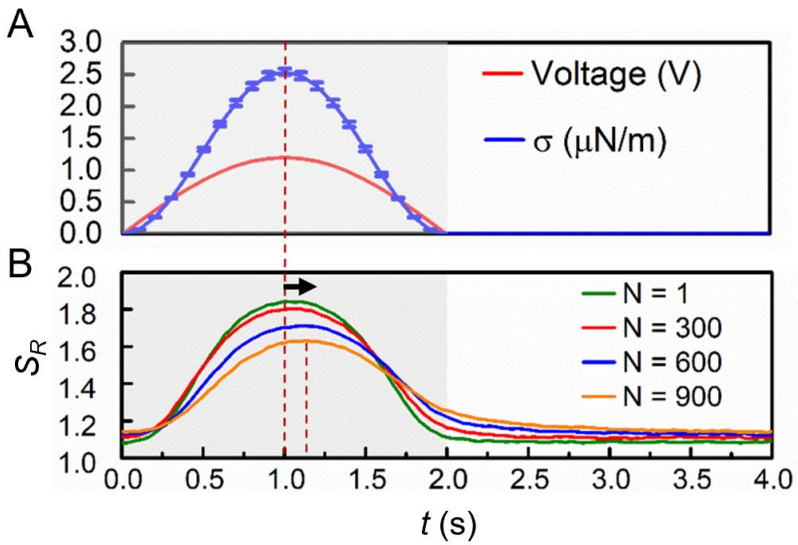

Fig. S6. An HWR sinusoidal waveform electrical excitation (red curve) and consequent shear stress averaged from the number of fatigue cycles, N = 1, 300, 450, 600, 900 (blue curve). The vertical red dashed line indicates the location of the peak value of voltage and membrane stress. (B) Instantaneous S_R averaged from individually tracked cells (n = 22) in both loading phase (gray region) and unloading phase (white region) at different fatigue cycles for the HWR sinusoidal waveform.

RBC Viability Assay

RBC viability was investigated by recourse to LIVE/DEAD® Viability/Cytotoxicity Kit (Invitrogen™ L3224, Thermo Fisher Scientific, Carlsbad, CA) staining of the green-fluorescent calcein-AM to indicate intracellular esterase activity. The assay was performed according to the manufacturer's protocol with a modification of the recommended buffer with DEP buffer, for which the osmotic pressure and pH value are similar to those of the cytoplasm of healthy RBCs. This replacement was done to ensure that no additional stress was imposed on the cells following fatigue testing. Cell viability results has been verified by identical viability results obtained for healthy RBCs prior to fatigue testing using the PBS buffer and the DEP buffer in parallel analyses. Considering the higher sample volume required by the LIVE/DEAD assay than the volume available (2.5 x10^{-6} mL) in the microfluidic device, we used a commercial 16-well plate (cat. No. 6324738001, ACEA Biosciences, San Diego, CA). The embedded interdigitated electrodes allowed us to obtain the required sample volume of RBCs (10 wells) that are subjected to simultaneous fatigue testing, equivalent to 1. 2 V–2 s loading and unloading as reported in the main paper. Each well was loaded with 200 μL of RBC suspension (10^6 cells/mL) in the DEP buffer and subjected to simultaneous cyclic electro-deformation for 1 h. The cyclic loading results of RBCs in the plate were consistent to the results obtained with cyclic loading our *in vitro* microfluidic device. Cells were collected after fatigue testing and stained with the viability assay, following the procedure stated in the manufacturer's protocol. Green fluorescence of the cells (Fig. S7A) was monitored by using a standard band pass filter with a wavelength of 475 nm, and compared to bright field image of the same of view of cells (Fig. S7B). Cell viability, defined as the percentage of cells that are viable, was not impacted by DEP buffer for long-term incubation under stationary condition. Initial cell viability before the fatigue testing was 100%. The fatigued RBCs showed an overall viability of 98±2% measured from 19 sets of fluorescence and bright field images.

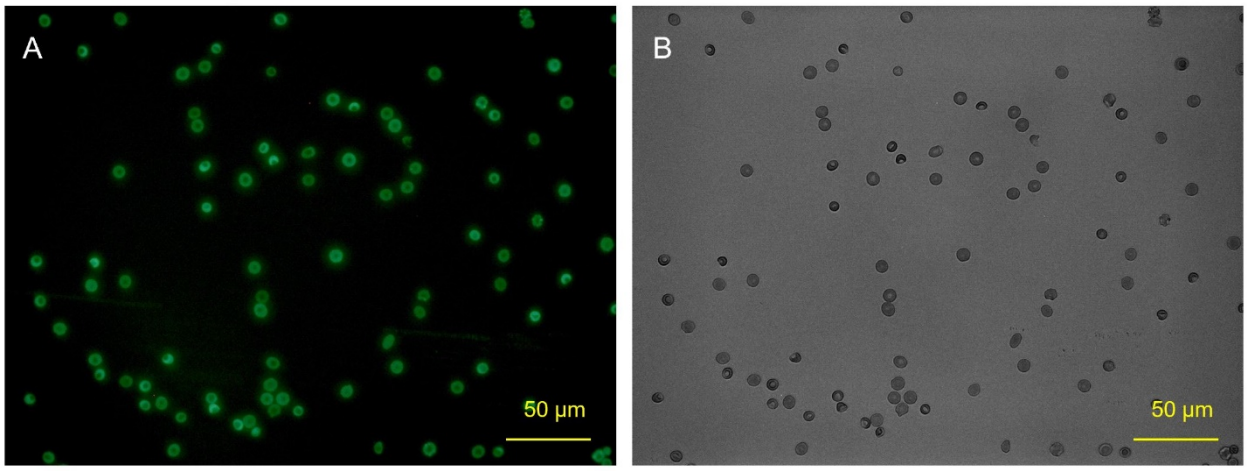

Fig. S7. RBC viability analysis by comparing the microscopic images of (A) green-fluorescent calcein-AM and (B) bright field image of the same field of view.

Axial versus Transverse Measurements of Deformation

As noted in the main paper, the principal extension ratio, $\lambda(t)$, was calculated by dividing the initial value of minor axis (b_0) by its transient value ($b(t)$). This choice of definition, instead of choosing the axial extension ratio, $a(t)/a_0$, was based on the consideration that a small part of deformed membrane along the tensile loading axis, *a,* is necessarily obstructed from view by the gold electrode when imaging the cell. This partial obstruction of view while imaging could have led to some errors in determining the extension ratio had $\lambda(t)$ been defined in terms of the relative stretch along the axial direction. We have determined experimentally that the choice of either of the two foregoing definitions would have absolutely no bearing on the trends and conclusions reported in this work. As expected, however, there are some differences in the results between these two related definitions of $\lambda(t)$, which stem from normal variations in cell responses in the two principal directions and differences in the accuracy of optical imaging between the two directions.

Fig. S8 demonstrates how the results presented in Fig. 4A would change had the extension ratio been defined as $\lambda(t) = a(t)/a_0$, instead of as $\lambda(t) = b_0/b(t)$, for static and cyclic loading. Here, Fig. S8A replots the results of Fig. 4A showing the variation of $\lambda^*_{\max}$ as a function of time for 1.2 V static loading and 1. 2 V–2 s for cyclic loading for $\lambda(t) = b_0/b(t)$, and compares it to the results, shown in Fig. S8B, for the same conditions with $\lambda(t) = a(t)/a_0$. It is evident here that the greater loss of deformability under cyclic loading is demonstrated in both cases. Effects of the two different means of assessing $\lambda(t)$ on the characterized mechanical fatigue of RBCs under 1.2 V static loading (n = 20) and 1.2 V-2 s cyclic loading (n = 35) are illustrated in Fig. S9. The characteristic time of relaxation, t_c, also increases with increasing number of fatigue cycles (see Fig. S3), irrespectively of whether deformation is quantified in terms of axial extension ratio or transverse contraction ratio.

We conclude, based on the results of Figs. S8 and S9 and other detailed results comparing the extension ratios in the two orthogonal directions, that estimates of principal deformation predicated either on the axial extension ratio, $a(t)/a_0$, or transverse contraction ratio, $b_0/b(t)$, has no effect on the trends discovered here about the role of mechanical fatigue in influencing the behavior of RBCs, despite some numerical differences in the extent of changes in behavior.

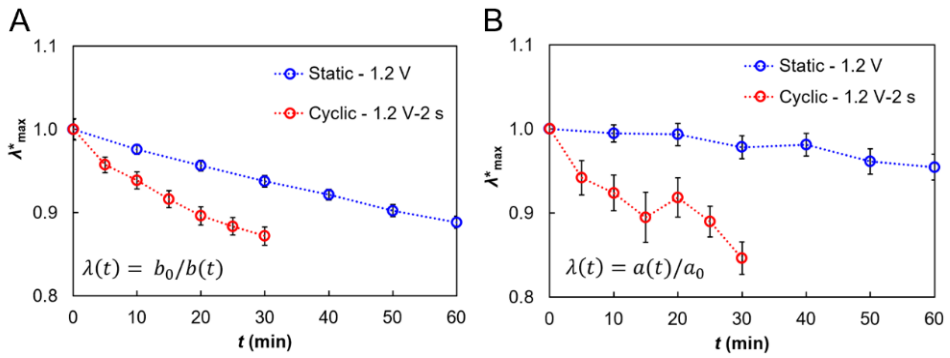

Fig. S8. A comparison of the static loading (n = 35) vs. cyclic loading (n = 20) effects on the deformability of RBCs using two different means of assessing the maximum extension ratio. (A) For $\lambda(t) = b_0/b(t)$, and (B) for $\lambda(t) = b(t)/b_0$. Error bars indicate SEM.

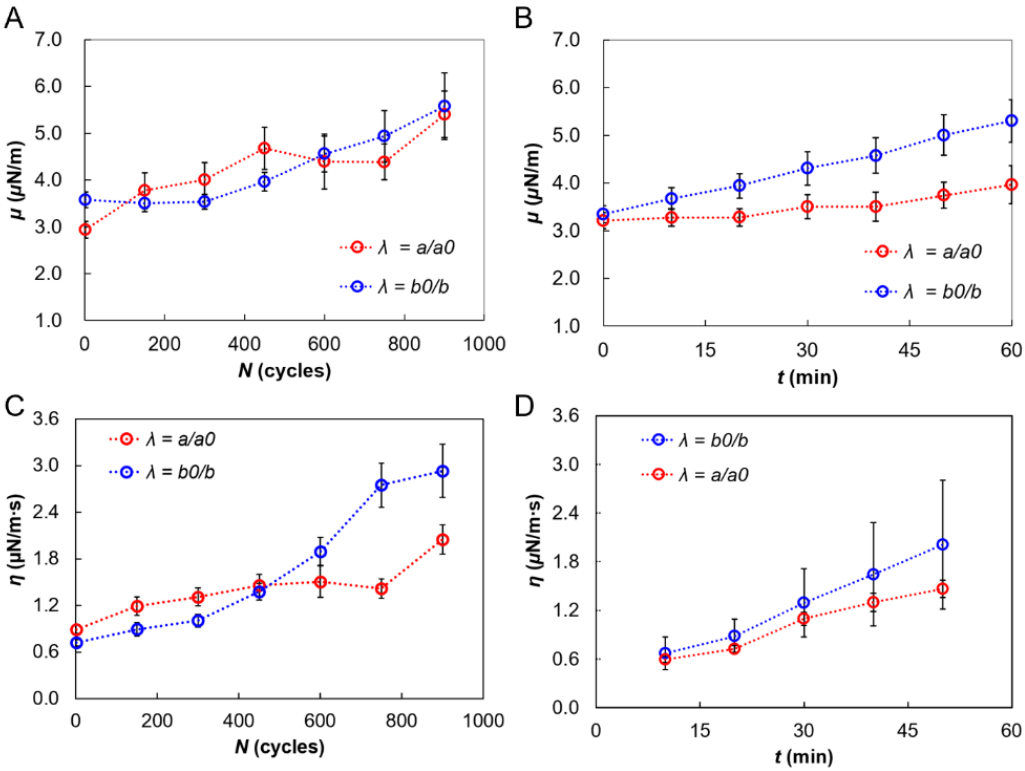

Fig. S9. Comparison between the two different means of assessing of the extension ratio, $\lambda(t) = b_0/b(t)$ and $\lambda(t) = a(t)/a_0$, for characterizations of (A) shear modulus, μ, under 1.2 V-2s cyclic loading, (B) shear modulus, μ, under 1.2 V static loading, (C) viscosity, η, under 1.2 V-2s cyclic loading, and (D) viscosity, η, under 1.2 V static loading. Error bars indicate SEM.

Movie S1. RBCs respond to a rectangular-waveform cyclic loading of 1.2 V with 2 s loading and 2 s unloading.

Movie S2. RBCs respond to static loading of 1.2 V.

Movie S3. Tank-treading motion of an RBC in response to the static loading of 1.2 V.

Movie S4. RBCs respond to an HWR sinusoidal-waveform cyclic loading of 1.2 V with 2 s loading and 2 s unloading.

References

1. Morgan H & Green NG (2003) *AC electrokinetics* (Research Studies Press).
2. Castellarnau M, Errachid A, Madrid C, Juarez A, & Samitier J (2006) Dielectrophoresis as a tool to characterize and differentiate isogenic mutants of Escherichia coli. *Biophysical journal* 91(10):3937-3945.
3. Zheng L, Brody JP, & Burke PJ (2004) Electronic manipulation of DNA, proteins, and nanoparticles for potential circuit assembly. *Biosensors and Bioelectronics* 20(3):606-619.
4. Thom F (2009) Mechanical properties of the human red blood cell membrane at -15 degrees C. *Cryobiology* 59(1):24-27.
5. Gascoyne P*, et al.* (2002) Microsample preparation by dielectrophoresis: isolation of malaria. *Lab on a Chip* 2(2):70-75.
6. Kumar S & Hesketh PJ (2012) Interpretation of ac dielectrophoretic behavior of tin oxide nanobelts using Maxwell stress tensor approach modeling. *Sensors and Actuators B: Chemical* 161(1):1198-1208.
7. Hochmuth RM, Worthy P, & Evans EA (1979) Red cell extensional recovery and the determination of membrane viscosity. *Biophysical journal* 26(1):101-114.
8. Evans EA & Hochmuth RM (1976) A solid-liquid composite model of the red cell membrane. *Journal of Membrane Biology* 30(1):351-362.